

# The Khuvsgul Earthquake of January 12, 2021 ( $M_W = 6.7$ , $M_L = 6.9$ ) and Early Aftershocks<sup>1</sup>

A. F. Emanov<sup>a,\*</sup>, A. A. Emanov<sup>a,c</sup>, V. V. Chechel'nitskii<sup>b</sup>, E. V. Shevkunova<sup>a</sup>,  
Ya. B. Radziminovich<sup>b,d</sup>, A. V. Fateev<sup>a,c</sup>, E. A. Kobeleva<sup>b</sup>, E. A. Gladyshev<sup>a</sup>,  
V. V. Arapov<sup>a</sup>, A. I. Artemova<sup>a</sup>, and V. G. Podkorytova<sup>a</sup>

<sup>a</sup> Altai–Sayan Branch, Federal Research Center “Geophysical Survey of the Russian Academy of Sciences,”  
Novosibirsk, 630090 Russia

<sup>b</sup> Baikal Branch, Federal Research Center “Geophysical Survey of the Russian Academy of Sciences,”  
Novosibirsk, 630090 Russia

<sup>c</sup> Trofimuk Institute of Petroleum Geology and Geophysics, Siberian Branch, Russian Academy of Sciences,  
Novosibirsk, 630090 Russia

<sup>d</sup> Institute of the Earth's Crust, Siberian Branch, Russian Academy of Sciences, Irkutsk, 664033 Russia  
\*e-mail: alex@gs.nsc.ru

Received April 10, 2021; revised June 10, 2021; accepted July 29, 2021

**Abstract**—The  $M_W = 6.7$ ,  $M_L = 6.9$  Khuvsgul (Khubsugul, Khövsgöl) earthquake occurred on January 12, 2021 in the Northern Mongolia close to the border of Russia. The earthquake caused ground shaking which reached intensity IX at the epicenter and was perceptible in the cities and villages of the Eastern and Western Siberia. The earthquake occurred in the region of the same-name fault and caused intense aftershock process on a segment between two fault's bends. The fault segment encompassed by the aftershocks goes from the lake to the northwest. Seismic activation has involved a segment of the boundary of the ancient Tuva–Mongolian microcontinent hosting the parallel Khuvsgul and Darkhat rift depressions and the Busingol rift depression consisting of three linearly elongated troughs. Until the present, the region of the Busingol depression was distinguished by high seismicity, whereas the regions of the Darkhat and Khuvsgul depressions were characterized by moderate and low seismicity, respectively. The earthquake of 2021 is the largest earthquake that occurred on the Khuvsgul fault over the entire history. In less than two months, the level of the frequency–magnitude graph for the aftershocks has exceeded the level of the annual frequency–magnitude graph of the earthquakes for the Altai–Sayan mountain region. The aftershock density is nonuniformly distributed along the fault; the structure of the distribution is correlated to the unilateral block structure of the Earth's crust east of the activated fault segment. The seismic potential of the Khuvsgul fault was estimated at  $M_{\max} = 7–7.5$ , and this earthquake, as suggested by the geological data, is not the maximum possible event. Given that seismic activation after the 1991 Busingol earthquake has not yet ceased, we have two strong activations in the Tuva–Mongolian block which can significantly affect evolution of its seismicity.

**Keywords:** Khuvsgul earthquake, strong motion, intensity, Altai–Sayan mountain region, Northern Mongolia, rift depression, seismic activation, aftershock process

**DOI:** 10.1134/S1069351322010025

## INTRODUCTION

The  $M_L = 6.9$  Khuvsgul earthquake of January 12, 2021 occurred on the eastern boundary of the Tuva–Mongolian block and caused an intense aftershock process. This block experiences uplifting; at the same time, rift depressions are confined to it (*Aktual'nye ...*, 2005; Levi et al., 2009; Sankov et al., 2003). Until the 2021 earthquake, such a strong seismic event has never occurred in the region of the western margin of Lake

Khuvsgul. The seismological network of the stations continuously recording the Earth's ground motion and transferring the data to the processing centers in Novosibirsk, Irkutsk, and Ulan-Bator is shown in Fig. 1.

From Fig. 1 it can be seen that a total number of stations is large but no stations are close to the epicenter. This impedes the determination of the source depth of both the main event and its aftershocks. In this situation, only the depth estimate is given at which we obtain the minimum residual of the determination of epicenter's coordinates. The minimum residual was obtained with a source depth of the main shock at 8 km.

<sup>1</sup> A year ago, on January 12, 2021, a strong earthquake occurred near Lake Baikal in the region of Lake Khuvsgul, Mongolia. In this issue of *Izvestiya, Physics of the Solid Earth*, we publish two papers devoted to this earthquake.

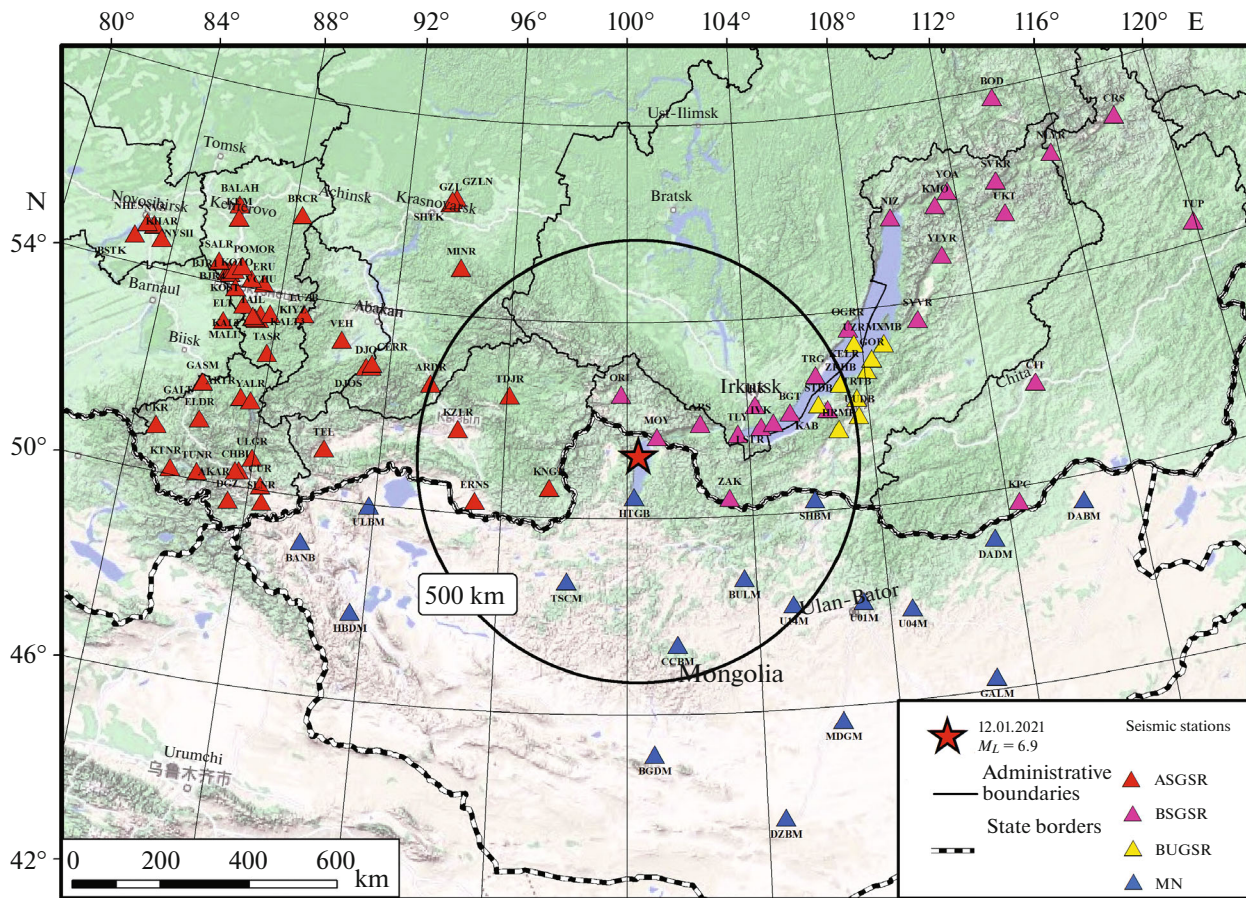


Fig. 1. Map of seismological network stations and epicenter of  $M_L$  6.9 Khuvsgul earthquake of January 12, 2021.

Seismic data processing includes three steps: automated determination of the parameters of a seismic event; preprocessing; and final processing using all the existing data. All types of the processing at the Center are conducted using the SeisComP3 software package (Weber et al., 2007; Hanka et al., 2010). SeisComP3 is designed to determine the entire range of basic parameters of seismic events: hypocenter location, energy estimates, focal mechanisms, etc. The software package also provides a wide range of possibilities to estimate the quality of the calculated parameters of seismic events.

The epicenter location is calculated using LocSat program (Bratt and Bache, 1988) in the global IASPEI91 velocity model (Kennet, 1991).

Overall, the center receives data from ~300 stations all over the world.

#### AFTERSHOCKS OF THE KHUVSGUL EARTHQUAKE

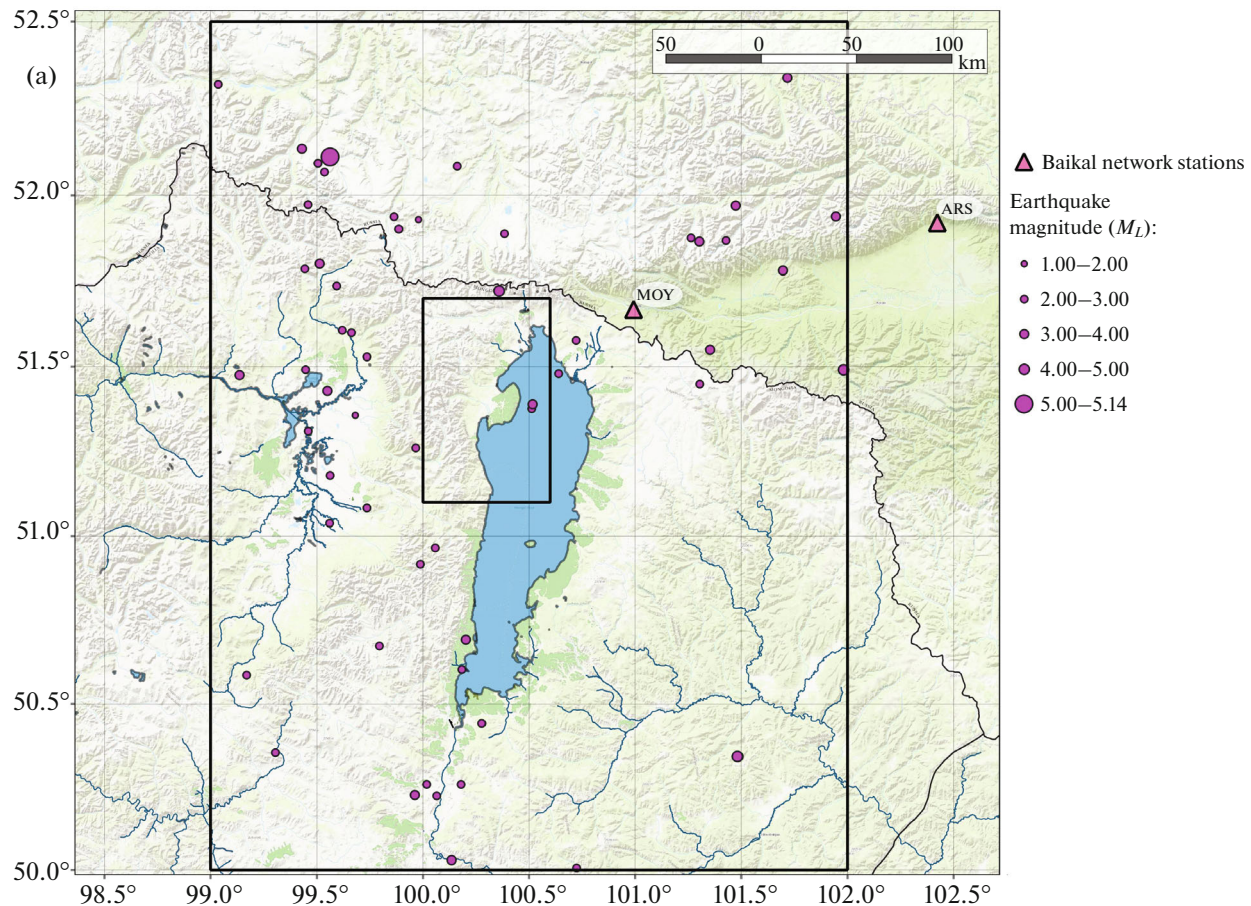
Figure 2a shows that in the previous year, there was almost no seismic activity in the epicentral region (indicated by the small box).

Figure 2b shows the map of the aftershocks of the Khuvsgul earthquake that occurred during the first month after the main shock. Within the larger box there are 4900 events and within the smaller box 4556 events.

It is clear that we mainly observe the development of the aftershock process along the fault zone; however, the seismic process has also involved the regions extending beyond the fault zone itself.

The tectonic structure of the epicentral zone was considered in a number of works (*Aktual'nye ...*, 2005); the most detailed scheme of the fault network for the epicentral region is presented in (Parfeevets and San'kov, 2006). It is this layout of the faults that is combined with the aftershock density map in Fig. 4. The area of the circle in the map of the aftershock density is  $S = \pi R^2$  where  $R = 0.02^\circ$ .

The source region coincides with the tectonic deformation that goes away from Lake Khuvsgul and is the boundary of the Tuva–Mongolian block (micro-continent). The aftershock density along the activated region is nonuniform. This is apparently associated with the presence of the branch faults to the right and,



**Fig. 2.** Map of epicenters of Khuvsgul earthquake, its aftershocks, and insignificant background seismicity (a) from January 1, 2020 to January 11, 2021; (b) from January 11, 2021 to February 10, 2021. Boundaries of boxes are selected in accordance with coverage by aftershock seismicity from Khuvsgul earthquake (small box) and with presence of earthquake epicenters in closest vicinity of aftershock process during 2020–2021 (large box). Negative earthquake magnitudes were detected close to MOY station (at distance of ~6.7 km) of Baikal network; events did not pertain to closest zone of aftershock activity.

as a consequence, complex block structure of the crust in the activated region.

It would seem that the main event is located in the margin of the seismically activated region; however, this question is a subject of additional studies because of the complexity of the records of the onset of the main shock.

Figure 4 shows the development of the aftershock process over time with the events projected to the fault line. It is characteristic that the main event has seismically activated the aftershock region at once along its entire length, and even the aftershock with magnitude 6 has not resulted in the spatial development of the aftershock region. During the initial period, numerous earthquakes with magnitudes above 5 occur. Events with magnitudes above 4 continue to be observed also beyond the time interval shown in Fig. 4. Judging by the energy and number of the aftershocks, the aftershock process of the Khuvsgul earthquake releases high energy level.

Another representation of the evolution of the aftershock process over time which does not take into account the linear dimensions of the activated region is shown in Fig. 5. The diagram in the magnitude–time coordinates reflects all the earthquakes from the smaller box in Fig. 2b.

The rate of aftershocks (the number of aftershocks per unit time) and the number of the earthquakes with maximum energies indicate that the aftershock process slowly decays with time. We have fully processed the aftershocks for January and February 2021; however, as can be seen in Fig. 5, practically no earthquakes with magnitudes below 1–1.5 are present in the aftershock process. This is most likely to be due to the incomplete recording in the epicentral region.

Earthquake recording in this region can be considered complete starting from  $M_L = 2–2.5$ . This estimate of the completeness is based on the size of the linear segment in the frequency–magnitude relationship of the earthquakes (Fig. 6).

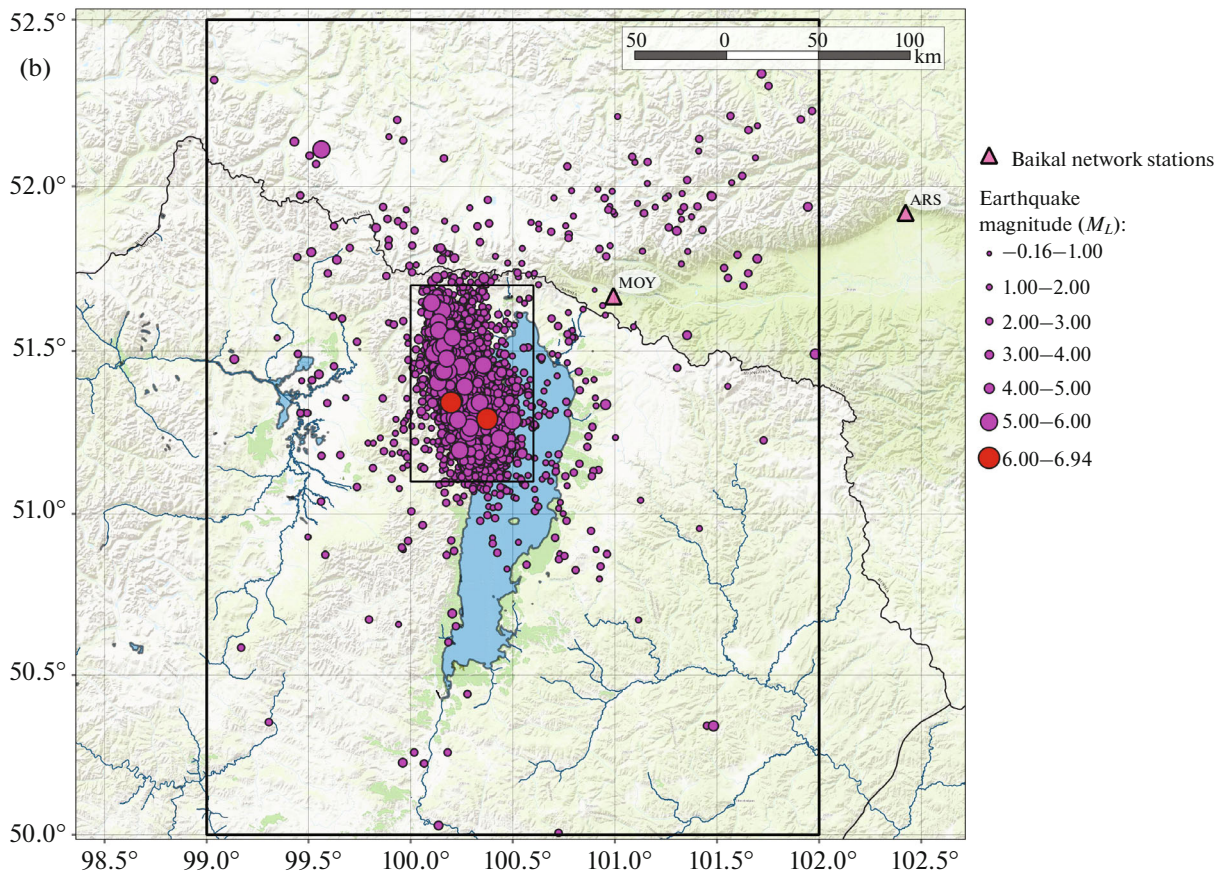


Fig. 2. (Contd.).

Figure 6 shows the frequency–magnitude graph for the aftershocks of the Khuvs gul earthquake. Due to the high rate of the aftershock process, it was possible to accumulate within two first months a sufficient number of the events for obtaining a log-linear frequency–magnitude distribution typical of a period of steady seismicity. The aftershock activity in the epicentral region is continuing and, judging by the aftershocks of the other earthquakes in Central Asia, can continue for years and even decades (Oparin et al., 2008). At the same time, the seismic process caused by the 1991 Busingol earthquake continues up to this day in the form of pulsing activation. The active period of the aftershock process of the Ureg–Nur earthquake lasted about five years and developed with the activation along a transverse fault, which resulted in the substantial deviation from the Omori law for the aftershock process overall. The aftershock activity of the 2003 Chuya earthquake continues up to the present and involves activation of the adjacent geological structures up to the occurrence of the new large earthquakes (Aigulak earthquake of 2019) giving rise to the strong aftershock processes (Emanov et al., 2021).

The Gutenberg–Richter  $b$ -value ( $-0.72$ ) is close to that in the similar relation for the Sayan–Altai

region based on the entire historical and instrumental data ( $-0.77$ ) and fully coincides with the  $b$ -value for the seismicity in the Altai–Sayan region for 2016.

The location of hypocenters and determination of the focal mechanisms of the earthquakes were carried out using modern software packages based on the up-to-date methods of digital data processing. Namely, this is the Hypoinverse-2000 software for event location in the multilayer velocity model and the FPFIT software for the calculation and visualization of the focal mechanisms of the earthquakes.

The Hypoinverse-2000 has several specific features. In particular, it includes a module of distance-based weighting which changes the weights of the phases depending on the obtained residuals. As the event location procedure only uses the first arrivals, the program is well suited for determining the hypocenters based on the data of local networks. In cases when the vicinity of earthquake epicenter is fairly densely covered by seismic stations, most other programs yield comparable results. Main discrepancies are observed in the case when there are insufficient stations and they nonuniformly cover the epicentral region. Thus, the accuracy of the absolute location of the epicenter is determined by several factors: the

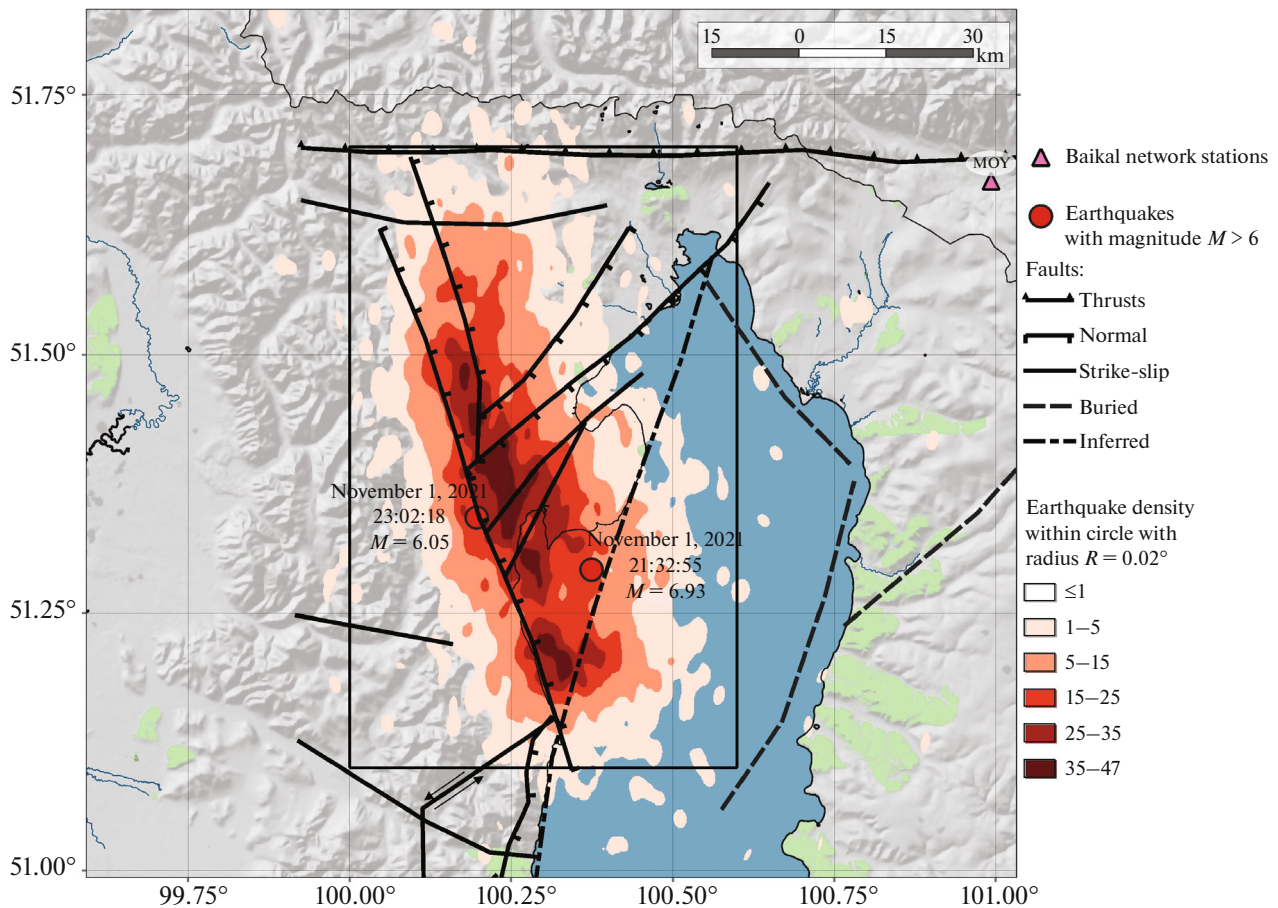


**Fig. 3.** Map of aftershock density of Khuvsgul earthquake over January–March 2021. Faults are indicated in accordance with (Parfeevets and Sankov, 2006).

geometry of the observational network, the arriving phases, the arrival-time picking accuracy, and knowledge of the velocity model of the crust. When determining the accuracy of the source depth, the last factor among the above ones is most significant.

The main parameters of the focal mechanisms of the earthquakes (the positions of two nodal planes and stress axes) are determined from the first-motion polarities using FPFIT software designed by P. Reasenberg and D. Oppenheimer (USGS). “The FPFIT software finds the double-couple solution to construct the fault plane which best fits the series of observations of the first-motion polarities for an earthquake. The inversion is accomplished through a two-step grid search procedure minimizing the normalized weighted sum of discrepancies in the first-motion polarities.” (Reasenberg and Oppenheimer, 1985). The minimization includes two weighting factors: one reflecting the supposed variant of the data and another based on the absolute value of the theoretical amplitude of P-wave discrepancy. The last weighting yields the least weight for the observations in the vicinity of the nodal planes. In addition to finding the solution with the minimum discrepancy, FPFIT finds an alternative

solution that also corresponds to the minimum discrepancy. The specific solution can only be selected after the analysis of the probable data errors, the unaccounted refractions, and the a priori known tectonic setting. For each constructed focal mechanism, FPFIT formally estimates the error in the parameters: in the strike azimuth, dip angles, and the slips of the nodal planes.

Figure 7 shows the focal mechanisms of the aftershocks that occurred before March 1, 2021 and for which the most reliable data on the orientations of the nodal planes have been obtained. The main event is almost pure normal fault but only with a small strike-slip component. The tension axis is horizontal and the pressure axis is gently inclined, which is quite consistent with the existing tectonic setting of rifting in the region of the Khuvsgul depression. The obtained mechanisms are comparable with the mechanisms determined by other organizations (Table 1). The mechanisms of the strongest aftershock with  $M = 6$  also has a significant normal fault component which practically passes into vertical normal faulting without horizontal extension, whereas the weaker events reflect stress redistribution on the branch faults and on

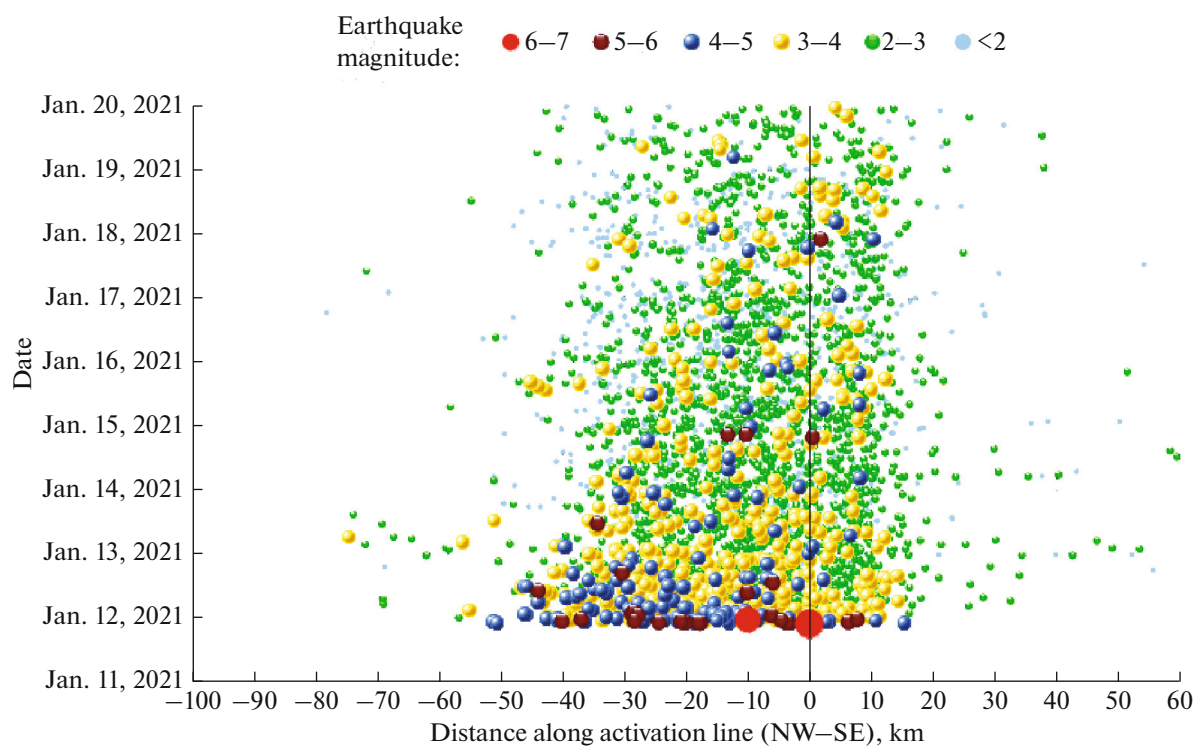


Fig. 4. Development of aftershocks (the latter are reduced to the line along fault zone).

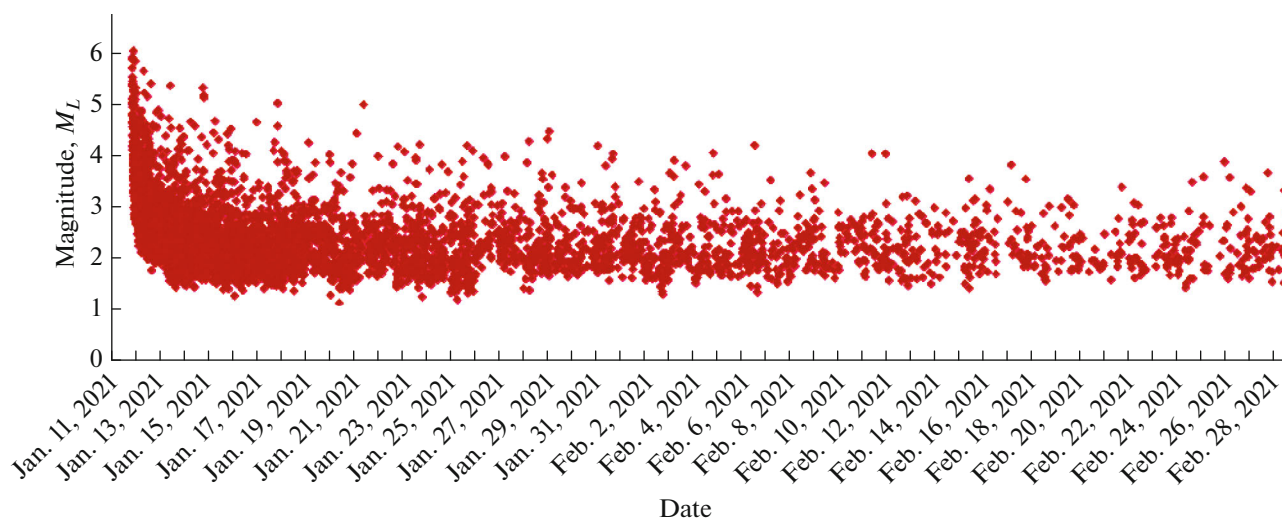


Fig. 5. Development of aftershock process of Khuvsgul earthquake over time.

the lower-order block structure, and their focal mechanisms are distributed more chaotically.

#### TECTONICS AND PREVIOUS SEISMICITY OF THE EPICENTRAL REGION

In the seismicity analysis, the Khuvsgul graben system of Northern Mongolia as a whole is typically considered (Khilko et al., 1985; Kochetkov et al., 1993;

Molnar et al., 1995). It includes the seismicity of the Busingol graben composed of three linear depressions, the Darkhat graben, and the Khuvsgul graben.

The Khuvsgul neotectonic zone comprises the Khuvsgul depression, the Darkhat and Busingol depressions parallel to it, and the uplifts separating these depressions (Parfeevets and Sankov, 2006). The Lake Khuvsgul depression is a half-graben with a steep western and a gently sloping eastern wall. The walls of

the Khuvsgul depression are framed by the faults of different orientation. The stress-tensor analysis based on the geological data characterizes this region as a zone of transpression (compression with shear) (Parfeevets and Sankov, 2006).

The map in Fig. 8 shows epicenters of the earthquake with  $M \geq 4$  that occurred in the Khuvsgul zone. The largest earthquakes closest to the epicenter are the 1950 Mondy and the 1991 Busingol earthquakes with magnitudes 7.0 and 6.5, respectively. The Mondy earthquake occurred in the structure of the Tunkin (or Tunka) Depression where, according to the geological data, the strike-slip displacement components combine with or even dominate the normal-fault components (Molnar et al., 1995). The Mondy earthquake is spatially close to the Khuvsgul earthquake but it occurred in a different structure and in the different stress conditions. The 1991 Busingol earthquake hit within the Tuva–Mongolian block in the system of rift depressions of Northern Mongolia. This earthquake was followed by the intense pulsing aftershock process that has been going on for almost three decades (Emanov et al., 2005; 2006). However, the main shock has not occurred on the main Busingol fault stretching along the depression of the same name but on a branch fault going into the Shishkhiid Plateau. The pulsing regime is associated with the propagation of the activation along the branch fault off the Busingol depression (Emanov et al., 2010).

Before the Khuvsgul earthquake, no large events and intensely developing seismic activations were observed within the Darkhat depression and the Khuvsgul depression. The Darkhat depression is host to the earthquakes with  $M = 4$ . Within the Khuvsgul depression, rare earthquakes with magnitude 5 were observed in the northern and southern parts, whereas the central part of the depression and, particularly, the epicentral zone of the 2021 earthquake were seismically not active.

The region of the aftershocks of the 2021 Khuvsgul earthquake covers the fault going toward northwest from the lake. The diversity of the focal mechanisms of the aftershocks is associated with a complex fault network in the epicentral zone and different orientations of the faults (Fig. 4) (Parfeevets and Sankov, 2006).

The block structure of the epicentral zone is presented in (Sankov et al., 2003). The aftershock process covers the region of the interblock fault exactly within the segment where the block boundary goes off Lake Khuvsgul towards the northeast. It should be noted that the velocity field of recent movements for the epicentral zone is rather low. Based on the studies (Sankov et al., 2003) it is stated that the collision of Hindustan and Eurasia only determines the part of the intra-continental deformations that is localized west of the  $105^\circ$  E meridian. The main change in the directions of GPS surface displacement vectors occurs in the interval  $98^\circ$ – $102^\circ$  E (Lukhnev et al., 2010).

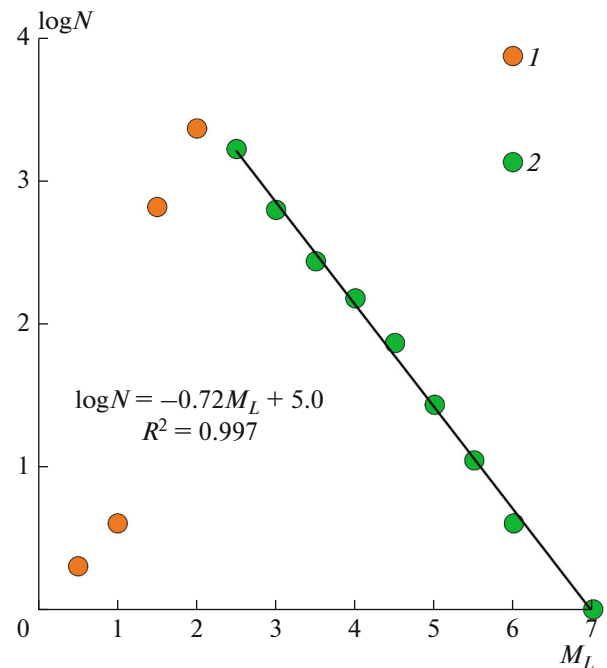
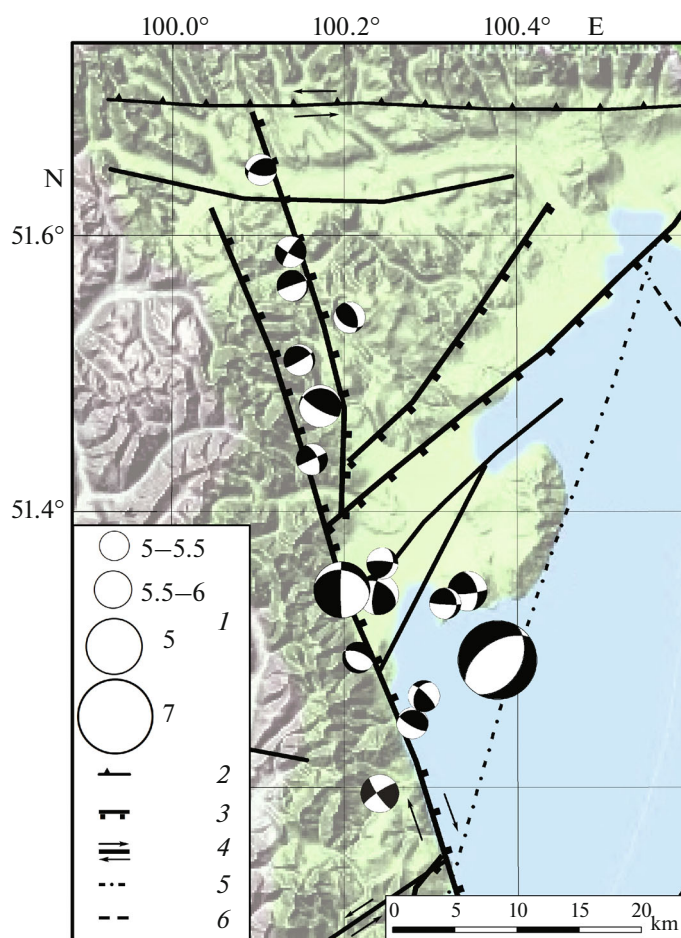


Fig. 6. Frequency–magnitude graph of earthquakes in region of Lake Khuvsgul over period from January 1 to February 28, 2021. (1) incomplete data; (2) complete data.

For the region of the Khuvsgul depression, based on the analysis of the seismological and geological data, a model is created and physical modeling is carried out to refine the stress state and the pattern of its evolution (Sankov et al., 2003; Parfeevets and Sankov, 2006). Based on the seismological data it was established that seismicity is characteristic of the northern part of the Khubsuigul depression and the zone of the latitudinal Ikhkhorogol–Mondy fault to its eastern continuation, as well as of the southern termination of the Khuvsgul depression. The crustal block containing rift depression of Northern Mongolia is dominated by transpression (compression with shear). Extensional conditions are established in the north of the Khuvsgul depression, and compressional conditions, in the southern end of the depression (Sankov et al., 2003). The Ikhkhorogol–Mondy fault is mainly characterized by the strike-slip type of focal mechanisms (Misharina et al., 1983).

The territory of the Northern Mongolia has been studied by paleoseismological methods (Khilko et al., 1985; Kochetkov et al., 1993; Misharina et al., 1995). In the epicentral region of the Khuvsgul earthquake, no signs of strong previous earthquakes have been revealed based on both paleogeological data and seismological observations (Kochetkov et al., 1993). In 1986–1987, the network of temporary stations recorded several weak earthquakes on the fault that hosted the 2021 earthquake considered in this work (Kochetkov et al., 1993). Overall, Kochetkov et al.



**Fig. 7.** Focal mechanisms of main shock and some aftershock of Khuvsgul earthquake. Stereograms of focal mechanisms are shown in projection on lower hemisphere: (1) magnitude; (1–6) neotectonic faults according to (Parfeevets and Sankov, 2006): (2) thrusts; (3) normal faults; (4) strike-slip faults; (5) hidden; (6) inferred.

**Table 1.** Focal mechanism parameters of the sources of the Khuvsgul earthquake of January 11, 2021 according to the data of the Altai–Sayan Branch of the Federal Research Center “Geophysical Survey of the Russian Academy of Sciences” (ASB FRC GS RAS) and international centers

No.	Center	Date	To, hh:mm:ss	Hypocenter			$M_W$	Nodal lanes						Stereogram
				$\phi_0$ N	$\lambda_0$ E	$h$ , km		NP1			NP2			
								STK	DP	SLIP	STK	DP	SLIP	
1	IPGP	11.01.2021	21:32:58	51.241	100.443	13	6.84	237	62	–52	358	46	–139	
2	USGS	11.01.2021	21:32:59	51.281	100.438	11.5	6.74	16	32	–110	219	60	–78	
3	Geofone	11.01.2021	21:32:59	51.21	100.47	18	6.7	226	51	–60	4	47	–121	
4	ASB FRC GS RAS	11.01.2021	21:32:58	51.13	100.28	8	6.7	30	40	–110	235	53	–74	



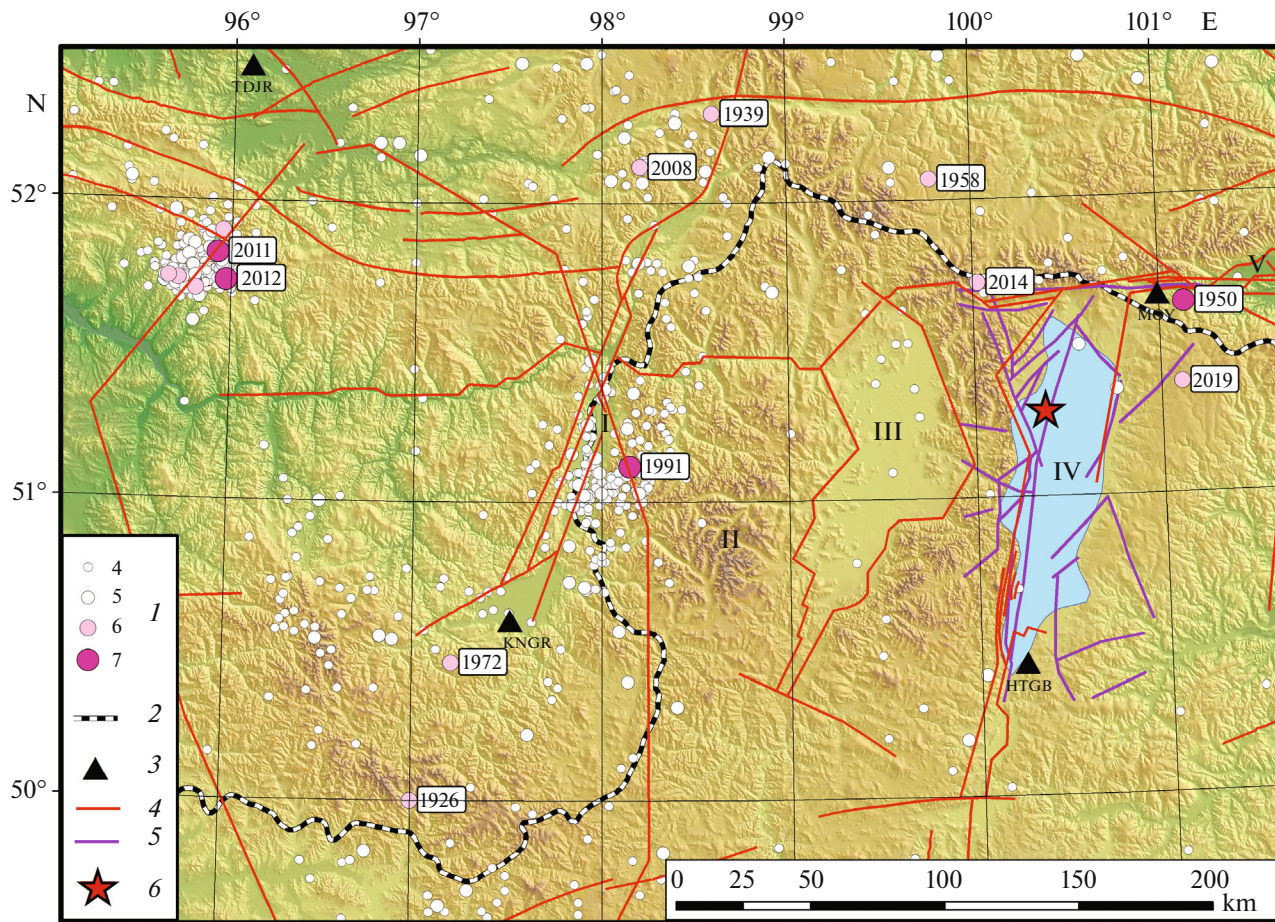


**Fig. 8.** Map of large earthquakes within Tuva–Mongolian block before 2021 Khuvsgul earthquake: (1) magnitude; (2) state border; (3) seismic station; (4) neotectonic fault according to (Trifonov, 1999); (5) neotectonic fault according to (Parfeevets and Sankov, 2006); (6) epicenter of  $M_L$  6.9 Khuvsgul earthquake of January 12, 2021. Roman numerals: I, Busingol graben; II, Shishikhid plateau; III, Darkhat graben; IV, Khuvsgul graben; V, Tunkin depression.

(1993) characterize the seismicity of the Tuva–Mongolian block as follows. Within the block, two latitudinal seismic zones are distinguished: the northern zone stretched along the Tunkin depression and the southern zone corresponding to the Bolnai fault parallel to the northern zone. Three submeridional rift depressions extend in the North–South direction from the northern to the southern sublatitudinal zone. The Busingol system of depressions is seismically active, especially after the Busingol earthquake of 1991. The Darkhat depression is characterized by weak seismicity along the central part of the depression. The Khuvsgul depression is practically aseismic relative the two structures parallel to it. In (Kochetkov et al., 1993) it was concluded that in the region of the Khuvsgul fault extended along the western wall of the depression of the same name, the process of energy accumulation takes place, and the occurrence of the large earthquakes along this fault is probable.

The data about the earthquakes presented in Fig. 8 are fully consistent with the results of the previous

works. By 2021, no significant changes in the seismicity of the structures in the region are observed compared to the 1990s.

The 2021 Khuvsgul earthquake caused seismic activation of one element of a long fault of the same name. The activated segment is located between two bends of the fault and spans the fault segment extending from the lake in the northwestern direction.

The system of rift depressions of the Tuva–Mongolian block holds a special place in the geodynamical processes of the Baikal Rift zone and Altai–Sayan folded area. If in the Altai–Sayan folded area earthquakes are concentrated in the mountain framing of the depression, then in the Baikal Rift zone they are predominantly occur within depressions (Emanov et al., 2005). The system of the Busingol depressions is characterized by the combination of seismicity within depressions and within their mountain framing, with alternating development of the seismic process (Emanov et al., 2006). The 1991 Busingol earthquake with  $M_s = 6.5$  occurred on a branch fault extending in

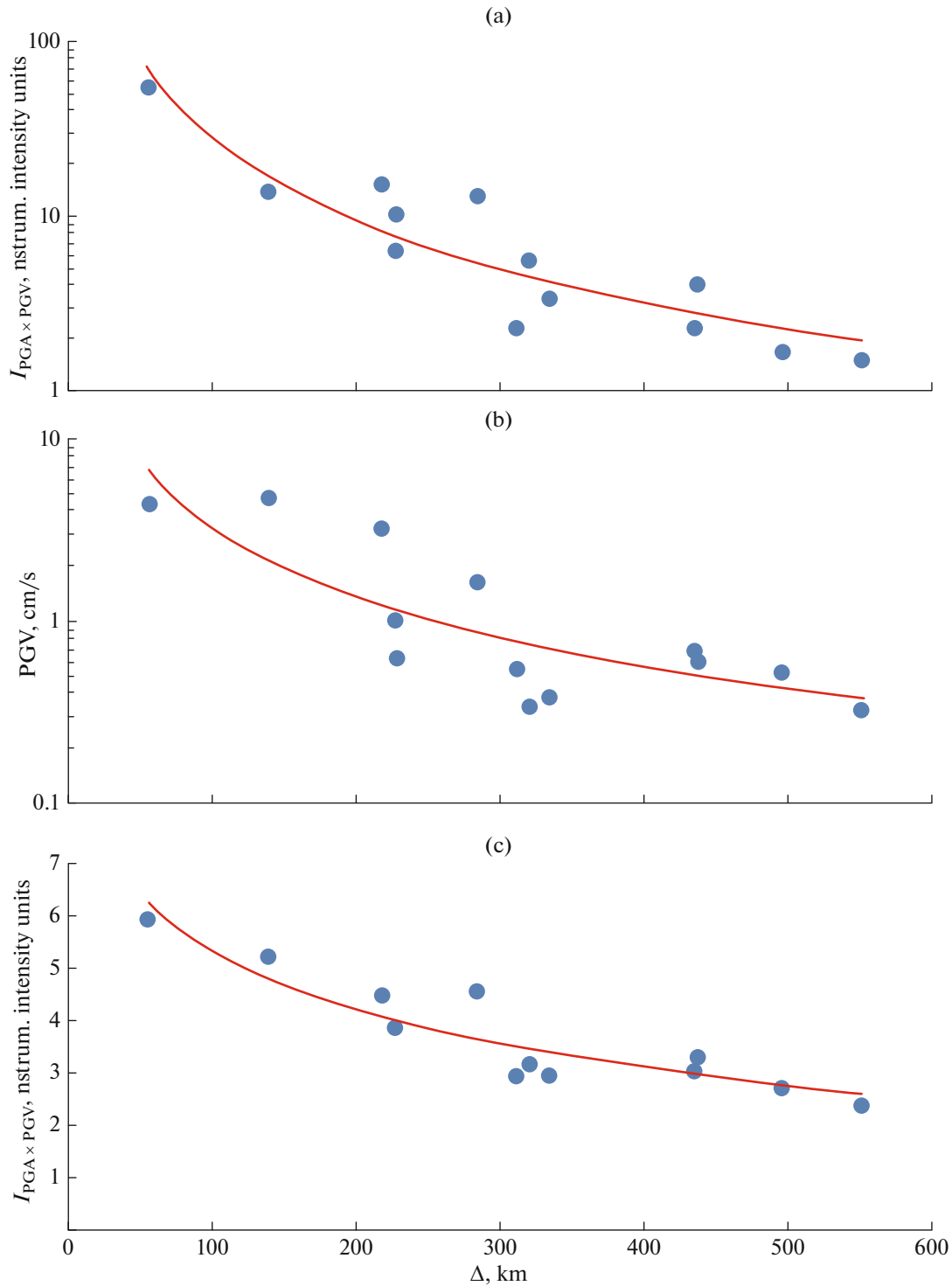


**Fig. 9.** Attenuation of (a) peak ground accelerations (PGA); (b) peak ground velocities (PGV), and (c) instrumental ground shaking intensity  $I_{PGA \times PGV}$  versus epicentral distance. Red lines correspond to regression equations (2)–(4).

the northeastern direction from the same name depression towards inside the Tuva–Mongolian block. It is the development of this fault that is a pulsing acti-

vation process which has been continuing for more than two decades (Emanov et al., 2010; 2021). The seismicity of the Darkhat depression, according to the

recent seismological observations, corresponds to the Baikal type of seismicity development (Emanov et al., 2005) when the depressions are active whereas the mountain framing is not (Florensov, 1978). The development of the aftershock process of the Khuvsgul earthquake follows the same pattern as that of the Busingol earthquake—from the depression towards its mountain framing, but in the northwestern direction.

### STRONG MOTION AND MACROSEISMIC DATA

The data on strong ground motion induced by the earthquakes with relatively high magnitudes are important for seismically active regions of Siberia, primarily for seismic hazard assessment and seismic zoning. Therefore, the strong Khuvsgul earthquake whose magnitude is estimated in the Global CMT Catalog at  $M_w = 6.7$  is of particular interest.

The strong motions from the Khubsuguil earthquake were recorded by the seismic stations of the Altai–Sayan and Baikal branches FRC GS RAS and by the stations of the Mongolian seismic network. The dynamic parameters of strong ground motion recorded at hypocentral distances ranging from 57 to 551 km are presented in Table 2.

The highest PGA value (54.6 cm/s<sup>2</sup>) was recorded by seismic station “Mondy” (MOY) at a distance of 57 km from the epicenter. Such PGAs are relatively rare for the South Baikal region, which makes the MOY record a substantial contribution to the strong motion database for East Siberia. As hypocentral distances increase, the recorded PGA and PGV values gradually decrease; and at a distance of 551 km, at Onguren station, the PGA value is as low as 1.5 cm/s<sup>2</sup> (Figs. 9a, 9b).

Interestingly, the PGA values at stations “Orlik,” “Kungurtug,” and “Irkutsk” are very close despite the substantial difference in the hypocentral distances 140, 218, and 284 km, respectively (Table 2, Fig. 9a). Besides the epicentral distance, the amplitudes of ground motion are also affected by soil conditions and the structure of the upper part of the section (Pavlenko, 2009; Kalinina et al., 2017; Graizer and Kalkan, 2016; Aleshin, 2017, etc.). The more intense ground motion at the stations “Irkutsk” and “Orlik” are probably associated with the peculiarities of frequency responses of the upper part of the section (Drennov et al., 2010). The relatively high PGA value recorded at station “Kungurtug” is probably due to the lower attenuation in the western azimuths from the epicenter. We also note that the maximum PGVs have been recorded by stations “Mondy” and “Orlik” (Fig. 9b). It can be hypothesized that the enhancement of ground motion at station “Orlik” is associated with the focal mechanism of the earthquake and determined by the directivity of seismic radiation from the source.

The frequencies corresponding to the maximum of the Fourier spectrum of accelerations ( $f_{SA}$ ) at the closest to the epicenter stations “Mondy” and “Orlik” are 4.1 and 3.9 Hz, respectively; at other stations,  $f_{SA}$  range from 1.3 to 2.8 Hz. The Russian Federation Building Regulation Code SP.286.1325800.2016 “Building Objects of High Criticality. Rules for Detailed Seismic Zoning” recommends estimating the dominant period  $T$  of accelerations using the following formula:

$$\log T = 0.15M_s + 0.25 \log R + C1 - 1.9 (\pm 0.2), \quad (1)$$

where  $R$  is the hypocentral distance, coefficient  $C1 = -0.20$  for underthrusts,  $-0.10$  for thrusts,  $0.00$  for strike-slip displacements and  $0.10$  for normal fault displacements.

The comparison shows that the dominant period of the accelerations  $T = 1/f_{SA}$  recorded in the Khuvsgul earthquake within the error agrees with the values calculated by formula (1) for normal faulting earthquakes with  $M_s = 6.7$  at ten stations; the discrepancy at MOY and ORL stations is 0.25 and 0.33 logarithmic units, respectively.

Based on the recorded PGA and PGV values, one can calculate instrumental shaking intensity from the product  $PGA \times PGV$ . In the opinion of F.F. Aptikaev and O.O. Erteleva, instrumental intensity  $I_{PGA \times PGV}$  is the best characteristic of seismic impact (Aptikaev and Erteleva, 2016). The PGA, PGV and  $I_{PGA \times PGV}$  dependences on hypocentral distance (Fig. 9) are described by the following regression equations:

$$\log PGA = 4.61 - 1.58 \log \sqrt{\Delta^2 + H^2} \pm 0.20, \quad (2)$$

$$\log PGV = 3.01 - 1.25 \log \sqrt{\Delta^2 + H^2} \pm 0.25, \quad (3)$$

$$I_{PGA \times PGV} = 12.9 - 3.77 \log \sqrt{\Delta^2 + H^2} \pm 0.50, \quad (4)$$

where PGA is the peak ground acceleration in cm/s<sup>2</sup>; PGV is the peak ground velocity in cm/s;  $\Delta$  is the epicentral distance in km; and  $H$  is the source depth in km. We note that to date, many formulas for estimating the amplitudes of velocities and accelerations in the different earthquake-prone regions depending on magnitude and distance have been proposed. The difference in the estimates based on different formulas can reach 100% (Steiberg et al., 1993), therefore it is preferable to use regional empirical equations.

The instrumental intensity estimates calculated from  $I_{PGV}$ ,  $I_{PGA}$ ,  $I_{PGA \times PGV}$  using formulas proposed in the new seismic intensity scale ShSI-17 (*GOST ...*, 2017) are presented in Table 2. In this context, it is interesting to compare the ground-shaking intensity estimates based on the instrumental records and the observed macroseismic effects.

The Khuvsgul earthquake was perceived over a very large area (Fig. 10) spanning the territory of North Mongolia and several objects of the Russian Federa-

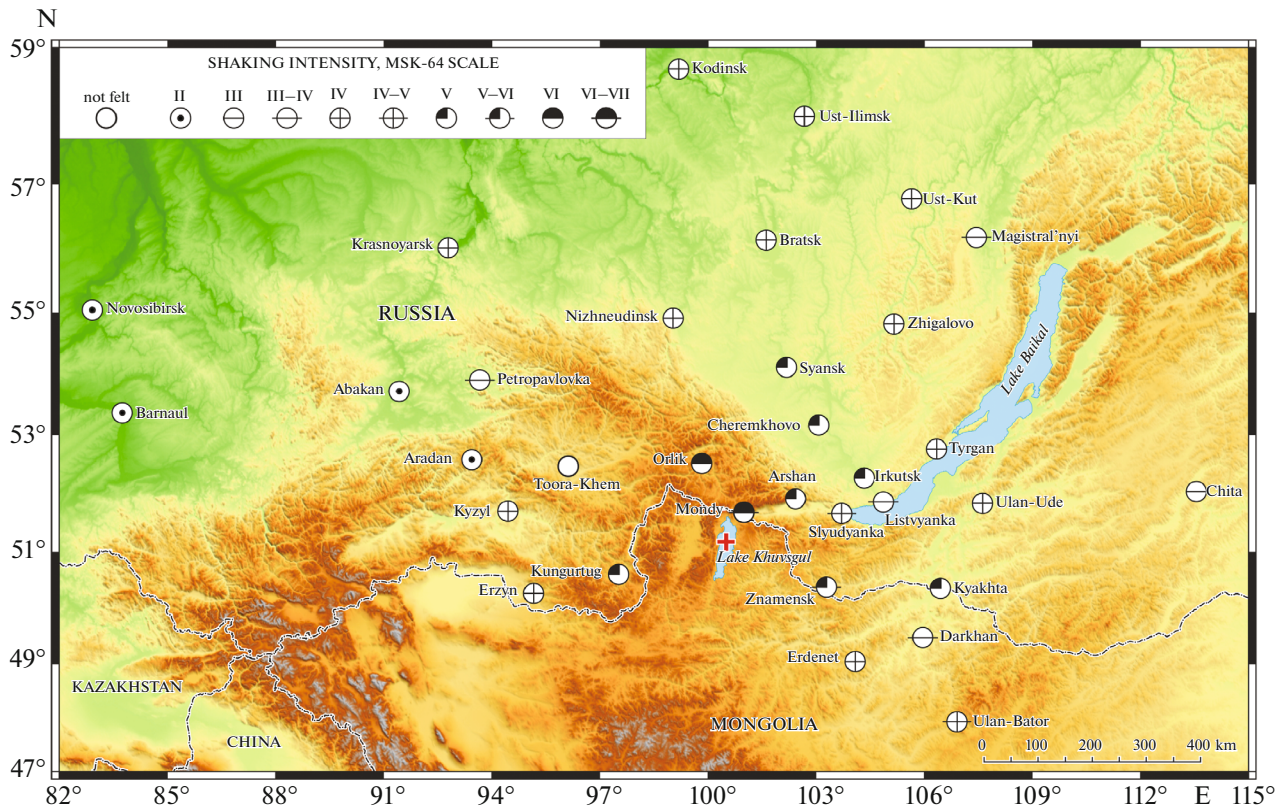


Fig. 10. Macroseismic manifestations of Khuvsgul earthquake of January 12, 2021. Red cross indicates instrumental epicenter.

tion. The maximum observed shaking intensity estimated at VI–VII was noted at Mondy at the epicentral distance of 57 km. To the west of the epicenter, perceptible ground shaking propagated to Novosibirsk (1230 km, intensity II) where it was felt on the upper floors of high-rise residential buildings. In the eastern direction, macroseismic effects of the earthquake are detected at a distance of 900 km in Chita (intensity III).

Together with the instrumental intensity estimates, Table 2 also shows the estimates based on the real macroseismic data. As follows from the presented data, the macroseismic effects observed at Orlik, Talaya, Irkutsk, and Tyrgan sites best agree with the instrumental intensity calculated from PGV. In these cases, the discrepancies are at most 0.5 of intensity unit. At Mondy and Aradan stations, the fullest correspondence between the instrumental and macroseismic estimates is observed with the PGA-based calculations. The instrumental intensity calculated from the  $\text{PGA} \times \text{PGV}$  product highly accurately coincides with the macroseismic estimate at the Kungurtug site; a good agreement in this case is also noted when using peak accelerations (PGA) alone. A relatively good consistency of the estimates is observed for the Listvyanka locality. The instrumental and macroseismic estimates agree worst at the town of Zakamensk where the discrepancy in the ground shaking intensity esti-

ated by different methods may reach one intensity unit. Overall, we may state a fairly good consistency between the instrumental and macroseismic intensity of shaking induced by the Khuvsgul earthquake. Thus, the obtained data support the applicability of the equations proposed in ShSI-17 scale for calculating shaking intensity from instrumental data in the conditions of South Siberia. However, making more substantiated conclusions requires further accumulation and comparison of the macroseismic information and the data on strong ground motions from the earthquakes in a wide range of magnitudes.

It is also interesting to compare ground motion attenuation in the case of the Khuvsgul earthquake with data for other relatively strong earthquakes in the Southern Baikal region. For instance, the attenuation of the ground motion induced by the Bystrinskoe earthquake ( $M_w = 5.5$ , n September 21, 2020) in the range of distances from 17 to 351 km is described by the following formulas (Gileva et al., 2020):

$$\log \text{PGA} = 4.67 - 1.75 \log \sqrt{\Delta^2 + H^2}, \quad (5)$$

$$\log \text{PGV} = 2.84 - 1.50 \log \sqrt{\Delta^2 + H^2}. \quad (6)$$

The slower attenuation of the ground motion from the Khuvsgul earthquake compared to that from the Bystrinskoe earthquake can be attributed to the lower

**Table 2.** Ground motion parameters and shaking intensity from the earthquake based on the instrumental data

Station	Code	$\Delta$ , km	Instrument	PGV, cm/s	PGA, cm/s <sup>2</sup>	$f_{SA}$ , Hz	$I_{PGV}$ , ShSI-17 scale	$I_{PGA}$ , ShSI-17 scale	$I_{PGA \times PGV}$ , ShSI-17 scale	$I_{macr}$ , macroscopic scale
Mondy	MOY	57	OSP-2M	4.35	54.60	4.1	6.1	6.2	5.9	VI–VII
Orlik	ORL	140	OSP-2M	4.75	13.90	3.9	6.2	4.7	5.2	VI
Kungurtug	KNGR	218	Guralp CMG-5T	3.19	15.20	2.8	5.8	4.8	5.0	V
Talaya	TAL	227	OSP-2M	1.01	6.40	1.6	4.8	3.9	3.9	IV–V
Zakamensk	ZAK	228	OSP-2M	0.62	10.30	4.2	4.3	4.4	3.9	V–VI
Irkutsk	IRK	284	Guralp CMG-5T	1.64	13.00	1.7	5.2	4.7	4.6	V
Listvyanka	LSTR	311	Guralp CMG-5T	0.55	2.30	1.7	4.2	2.8	2.9	III–IV
Todzha	TDJR	320	SKM	0.34	5.60	2.0	3.7	3.8	3.2	I
Tosontsegel	TSCM	334	Guralp CMG-6T	0.38	3.40	1.3	3.8	3.2	2.9	–
Tyrgan	TRG	435	OSP-2M	0.68	2.30	2.0	4.4	2.8	3.1	IV
Kabansk	KAB	437	OSP-2M	0.59	4.10	1.8	4.2	3.4	3.3	–
Aradan	ARDR	496	Guralp CMG-6T	0.52	1.66	2.0	4.1	2.4	2.7	II
Onguren	OGRR	551	OSP-2M	0.33	1.50	1.7	3.7	2.3	2.4	–

Detailed data on the subsoil, instruments, and coordinates of seismic stations are presented in (Zemletryaseniya ..., 2020). PGV are peak ground velocities; PGA are peak ground accelerations;  $f_{SA}$  is frequency corresponding to the maximum of the Fourier spectrum;  $I_{PGV}$ ,  $I_{PGA}$ ,  $I_{PGA \times PGV}$  is instrumental shaking intensity calculated from PGV, PGA and the product  $PGA \times PGV$ , respectively, using the equations proposed in ShSI-17 seismic intensity scale (GOST ..., 2017);  $I_{macr}$  is the shaking intensity from macroseismic data. Velocity waveforms from acceleration waveforms and vice versa are obtained by the integration and differentiation in frequency domain with the allowance for frequency responses of seismometer channels; the Fourier spectra are calculated in DeepSoil software (Hashash et al., 2020).

frequencies of the motions. The data suggesting an increase in the dominant period of the motions with magnitude are presented by many authors. For example, Graizer and Kankan (2007; 2009; 2011) analyzed the spectra of the earthquakes with magnitudes from 4.9 to 7.6 and established the shift of the dominant period from 0.15 to 0.5 s. The influence of structural peculiarities of the medium on the propagation of seismic oscillations is also not excluded.

Unfortunately, reliable information about macroseismic effects in the epicentral zone of the Khuvsgul earthquake is absent because the territory is unpopulated. Nevertheless, epicentral shaking intensity can be approximately estimated based on Eq. (4) and macroseismic field equation proposed by N.V. Shebalin (1972):

$$I_0 = bM - v \log H + c, \quad (7)$$

where  $I_0$  is the epicentral shaking intensity;  $M$  is earthquake magnitude;  $H$  is the source depth in km;  $b$ ,  $v$ , and  $c$  are empirical coefficients.

Assuming the magnitude  $M_S = 6.7$ , source depth  $H = 8$  km, and coefficients  $b$ ,  $v$  and  $c$  for the Baikal region equal to 1.5, 4, 4, respectively (Novyi ..., 1977), we obtain the intensity estimate  $I_0 = 10.4$  from the macroseismic equation (7) and 9.6 from Eq. (4). These values appear to be significantly overestimated and inconsistent with the real situation. If we assume the source depth at 14.3 km in accordance to GCMT, the epicentral intensity estimated from the macroseis-

mic equation will be 9.4 and that from Eq. (4) will be 8.6. Thus, the calculations of epicentral intensity show that the source depth of the earthquake appears to be underestimated.

The ground shaking intensity at the epicenter can also be calculated from the equation for the Mongolian–Baikal region proposed in (Seismicheskoe ..., 1977)

$$I_0 = 1.33M + 0.2. \quad (8)$$

Equation (8) provides a more realistic estimate according to which the epicentral intensity of the shaking is 9.1.

## CONCLUSIONS

– The  $M_W = 6.7$ ,  $M_L = 6.9$  Khuvsgul earthquake of January 12, 2021 occurred in the region of the same name fault and caused intense aftershock process on a fault segment between two bends. The fault segment encompassed by the aftershocks extends from the lake towards the northwestern direction.

– The seismically activated fault is characterized as the eastern boundary of the Tuva–Mongolian microcontinent associated with the formation of the system of subparallel rift depression perpendicular to the other depression of the Baikal Rift zone.

– According to the seismic zoning data, the fault is characterized as a zone of earthquake sources occurrence (earthquake source zone) prone to the earth-

quakes with magnitudes 7–7.5 (Kochetkov et al., 1993).

– Neither instrumental nor paleogeological data suggest high seismic activity in the epicentral zone of the Khuvsgul earthquake. Based on the analysis of seismicity evolution in the vicinity of the Bussingol and Darkhat rift depressions, the forecast about the preparation of a large earthquake in the region of the Khuvsgul fault was made (Kochetkov et al., 1993), which was validated by the 2021 earthquake.

– The aftershocks of only the first two months after the main shock (a total of ~5000 events) allow us to conclude that the areal development of the aftershocks is nonuniform and that there is a connection with the one-sided system of feathering (branch) faults which provides the block structure of the epicentral region.

– Based on the strong motion and macroseismic data for the Khuvsgul earthquake and based on the regional macroseismic equation for the Baikal Rift zone, the shaking intensity at the epicenter is estimated at 9. It is noted that the spatial attenuation of the ground motions from the 2021 Khuvsgul earthquake is slower than from the 2020 Bystrinskoe earthquake, which is due to the differences in the frequencies of oscillations.

#### CONFLICT OF INTEREST

The authors declare that they have no conflicts of interest.

#### OPEN ACCESS

This article is licensed under a Creative Commons Attribution 4.0 International License, which permits use, sharing, adaptation, distribution and reproduction in any medium or format, as long as you give appropriate credit to the original author(s) and the source, provide a link to the Creative Commons license, and indicate if changes were made. The images or other third party material in this article are included in the article's Creative Commons license, unless indicated otherwise in a credit line to the material. If material is not included in the article's Creative Commons license and your intended use is not permitted by statutory regulation or exceeds the permitted use, you will need to obtain permission directly from the copyright holder. To view a copy of this license, visit <http://creativecommons.org/licenses/by/4.0/>.

#### REFERENCES

- Aki, K. and Richards, P.G., *Quantitative Seismology, Theory and Methods*, in 2 vols., San Francisco: Freeman, 1980.
- Aktual'nye voprosy sovremennoi geodinamiki Tsentral'noi Azii* (Topical Issues of Modern Geodynamics of Central Asia), Levi, K.G. and Sherman, S.I., Eds., Novosibirsk: SO RAN, 2005.
- Aleshin, A.S., *Kontinual'naya teoriya seismicheskogo mikro-raionirovaniya* (The Continual Theory of Seismic Micro-zoning), Moscow: Nauch. mir, 2017.
- Aptikaev, F.F. and Erteleva, O.O., Russian seismic intensity scale of new generation, *Vopr. Inzh. Seismol.*, 2016, vol. 43, no. 2, pp. 43–52.
- Bachmanov, D.M., Kozhurin, A.I., and Trifonov, V.G., The active faults of Eurasia database, *Geodinam. Tektonofiz.*, 2017, vol. 8, no. 4, pp. 711–736.
- Bratt, S.R. and Bache, T.C., Locating events with a space network of regional arrays, *Bull. Seismol. Soc. Am.*, 1988, vol. 78, pp. 780–798.
- Dobrynina, A.A., Chechel'nitskii, V.V., and San'kov, V.A., Seismic quality factor of the lithosphere of the southwestern flank of the Baikal rift system, *Russ. Geol. Geophys.*, 2011, vol. 52, no. 5, pp. 555–564.
- Drennov, A.F., Dzhurik, V.I., Serebrennikov, S.P., and Drennova, N.N., Influence of the upper section on the amplitude-frequency content of a seismic signal by the example of seismic stations in Pribaikalye and Trans-Baikal area, *Seism. Prib.*, 2010, vol. 46, no. 2, pp. 15–25.
- Emanov, A.F., Emanov, A.A., Filina, A.G., and Leskova, E.V., Spatial-temporal features of seismicity in the Altai-Sayan mountainous region, *Fiz. Mezhomekh.*, 2005, vol. 8, no. 1, pp. 49–64.
- Emanov, A.F., Emanov, A.A., Filina, A.G., Leskova, E.V., Kolesnikov, Yu.I., and Rudakov, A.D., General and individual in the development of aftershock processes of the largest earthquakes in the Altai-Sayan mountainous region, *Fiz. Mezhomekh.*, 2006, vol. 9, no. 1, pp. 33–44.
- Emanov, A.F., Emanov, A.A., and Leskova, E.V., Seismic activations in the Belino-Busingol zone, *Fiz. Mezhomekh.*, 2010, vol. 13, no. S1 (Special Issue), pp. 72–77.
- Emanov, A.F., Emanov, A.A., Fateev, A.V., Soloviev, V.M., Shevkunova, E.V., Gladyshev, E.A., Antonov, I.A., Korabel'shchikov, D.G., Podkorytova, V.G., Yankaitis, V.V., Elagin, S.A., Serezhnikov, N.A., Durachenko, A.V., and Artomova, A.I., Seismological studies in the Altai-Sayan mountain region, *Ross. Seismol. Zh.*, 2021, vol. 3, no. 2, pp. 20–51.
- Florensov, N.A., *Ocherki strukturnoi geomorfologii* (Essays on Structural Geomorphology), Moscow: Nauka, 1978.
- Gileva, N.A., Kobeleva, E.A., Radziminovich, Ya.B., Melnikova, V.I., and Chechel'nitsky, V.V., The September 21, 2020,  $M_w=5.5$ , Bystraya earthquake in the Southern Baikal Region: preliminary results of instrumental and macroseismic observations, *Seism. Instrum.*, 2021, vol. 57, no. 2, pp. 173–186.
- <https://doi.org/10.3103/S0747923921020237>
- GOST (State Standard) P57546–2017: Earthquakes. Seismic Intensity Scale*, 2017.
- Graizer, V.M. and Kalkan, E., Ground motion attenuation model for peak horizontal acceleration from shallow crustal earthquakes, *Earthquake Spectra*, 2007, vol. 23, no. 3, pp. 585–613.
- <https://doi.org/10.1193/1.2755949>
- Graizer, V. and Kalkan, E., Prediction of spectral acceleration response ordinates based on PGA attenuation, *Earthquake Spectra*, 2009, vol. 25, no. 1, pp. 39–69.
- <https://doi.org/10.1193/1.3043904>
- Graizer, V. and Kalkan, E., Modular attenuation modeling, *Seismol. Res. Lett.*, 2011, vol. 82, no. 1, pp. 21–31.
- <https://doi.org/10.1785/gssrl.82.1.21>
- Graizer, V. and Kalkan, E., Summary of the GK15 ground-motion prediction equation for horizontal PGA and 5% damped PSA from shallow crustal continental earthquakes, *Bull. Seismol. Soc. Am.*, 2016, vol. 106, no. 2, pp. 687–707.
- <https://doi.org/10.1785/0120150194>
- Hanka, W. et al. (GITEWS Seismology Collab.), Real-time earthquake monitoring for tsunami warning in the Indian

- Ocean and beyond, *Nat. Hazards Earth Syst. Sci.*, 2010, vol. 10, pp. 2611–2622.
- Hashash, Y.M.A., Musgrove, M.I., Harmon, J.A., Ilhan, O., Xing, G., Numanoglu, O., Groholski, D.R., Phillips, C.A., and Park, D., “*DEEPSOIL 7.0, User Manual*,” Urbana: Board of Trustees of University of Illinois at Urbana-Champaign, 2020.
- IASPEI 1991 Seismological Tables*, Kennett, B.L.N., Ed., Canberra: Research School of Earth Sciences, Australian National University, 1991.
- Kalinina, A.V., Ammosov, S.M., Bykova, V.V., and Tatevosyan, R.E., On the applicability of standard response spectra for seismic hazard assessment, *Vopr. Inzh. Seismol.*, 2017, vol. 44, no. 2, pp. 61–73.  
<https://doi.org/10.21455/VIS2017.2-4>
- Khil’ko, S.D., Kurushin, R.A., Kochetkov, V.M., Misharina, L.A., Mel’nikova, V.I., Gileva, N.A., Lastochkin, S.V., Balzhinnyam, I., and Monkhood, D., *Zemletryaseniya i osnovny seismicheskogo raionirovaniya Mongolii, Tr. sovместnoi sovetско-mongol’skoi nauchno-issl. geol. ekspeditsii, vyp. 41* (Earthquakes and the Basics of Seismic Zoning in Mongolia, Tr. Joint Soviet-Mongolian Sci. Res. Geol. Expedition, vol. 41), Moscow: Nauka, 1985.
- Klein, F.W., *User’s Guide to HYPOINVERSE-2000, a Fortran Program to Solve for Earthquake Locations and Magnitudes*, U.S. Geological Survey, Open-File Report 02-171, 2002, 123 p.
- Kochetkov, V.M., Khil’ko, S.D., Zorin, Yu.A., Ruzhich, V.V., Turutanov, E.Kh., Arvisbaagar, N., Bayasgalan, A., Kozhevnikov, V.M., Erdenbeleg, B., Chipizubov, A.V., Monkhood, D., Anikanova, G.A., Klyuchevskii, A.V., Naidich, V.I., Bayar G., et al., *Seismotektonika i seismichnost’ Prikhubsugul’ya* (Seismotectonics and Seismicity of the Khubsugul Region), Novosibirsk: Nauka, 1993.
- Kuz’michov, A.B. *Tektonicheskaya istoriya Tuvino-Mongol’skogo massiva: rannebaikal’skii, pozdnebaikal’skii i rannekaledonskii etapy* (Tectonic History of the Tuva-Mongolian Massif: Early Baikal, Late Baikal and Early Caledonian Stages), Moscow: Probel-2000, 2004.
- Lahr, J.C., 1980, *HYPOELLIPSE: a computer program for determining local earthquake hypocentral parameters, magnitude and first motion pattern*, U.S. Geological Survey Open-File Report 80-59, 59 p.
- Levi, K.G., Sherman, S.I., and San’kov, V.A., Recent Geodynamics of Asia: map, principles of its compilation, and geodynamic analysis, *Geotectonics*, 2009, vol. 43, no. 2, pp. 152–165.
- Lukhnev, A.V., San’kov, V.A., Miroshnichenko, A.I., Ashurkov, S.V., and Calais, E., GPS rotation and strain rates in the Baikal-Mongolia region, *Russ. Geol. Geophys.*, 2010, vol. 51, no. 7, pp. 785–793.
- Misharina, L.A., Mel’nikova, V.I., and Balzhinnyam, I., Southwestern boundary of the Baikal rift zone according to the data on the mechanism of earthquake sources, *Vulkanol. Seismol.*, 1983, no. 2, pp. 74–83.
- Molnar, P., Kurushin, R.A., Kochetkov, V.M., Dem’yanovich, M.G., Borisov, V.A., and Vashchilov, Yu.Ya., Deformation and rupture formation during strong earthquakes in the Mongol-Siberian region, in *Glubinnoe stroenie i geodinamika Mongolo-Sibirskogo regiona* (Deep Structure and Geodynamics of the Mongol-Siberian Region) Logachev, N.A., Kochetkov, V.M., and Zorin, Yu.A., Eds., Novosibirsk: Nauka, 1995, pp. 5–55.
- Novoishaya tektonika, geodinamika i seismichnost’ Severnoi Evrazii* (The Latest Tectonics, Geodynamics and Seismicity of Northern Eurasia), Grachev, A.F., Ed., Moscow: PROBEL, 2000.
- Novyi katalog sil’nykh zemletryaseni na territorii SSSR s drevneishikh vremen do 1975 g.* (New Catalog of Strong Earthquakes on the Territory of the USSR from Ancient Times to 1975), Kondorskaya, N.V. and Shebalin, N.V., Eds., Moscow: Nauka, 1977.
- Oparin, V.N., Sashurin, A.D., Kulakov, G.I., Leontev, A.V., Nazarov, L.A., Nazarova, L.A., Tapsiev, A.P., Khachai, O.A., Khachai, O.Yu., Emanov, A.F., Emanov, A.A., Leskova, E.V., Kolesnikov, Yu.I., Nemirovich-Danchenko, M.M., Vostrikov, V.I., et al., *Sovremennaya geodinamika massiva gornyykh porod verkhnei chasti litosfery: istoki, parametry, vozdeistvie na ob’ekty nedropol’zovaniya* (Modern Approaches in Geodynamics of Rock Masses of the Upper Lithosphere: Origin, Parameters, Effect on Mineral Resource Development), Novosibirsk: SO RAN, 2008.
- Parfeevets, A.V. and San’kov, V.A., *Napryazhonnoe sostoyanie zemnoi kory i geodinamika yugo-zapadnoi chasti Baykal’skoi riftovoi zony* (Stressed State of the Earth’s Crust and Geodynamics of the Southwestern Part of the Baikal Rift Zone), Levi, K.G., Ed., Novosibirsk: Geo, 2006.
- Pavlenko, O.V., *Seismicheskie volny v gruntovykh sloyakh: nelineinoe povedenie grunta pri sil’nykh zemletryasenyakh poslednikh let* (Seismic Waves in Soil Layers: Nonlinear Behavior of Soil during Strong Earthquakes in Recent Years), Moscow: Nauchn. mir, 2009.
- Reasenber, P.A. and Oppenheimer, D., FPFIT, FPLOT, and FPPAGE: Fortran computer programs for calculating and displaying earthquake fault-plane solutions, U.S. Geological Survey, Open-File Report no. 85-739, 1985.
- San’kov, V.A., Lukhnev, A.V., Miroshnichenko, A.I., Levi, K.G., Ashurkov, S.V., Bashkuev, Yu.B., Dembelev, M.G., Calais, E., Deverchere, J., Vergnolle, M., Bechtur, B., and Amarjargal, Ch., Recent movements of the Earth’s crust in the Mongol-Siberian region inferred from GPS geodetic data, *Dokl. Earth Sci.*, 2003, vol. 393, no. 8, pp. 1082–1085.
- Seismicheskoe raionirovanie Vostochnoi Sibiri i ego geologofizicheskie osnovy* (Seismic Zoning of Eastern Siberia and Its Geological and Geophysical Foundations), Solonenko, V.P., Ed., Novosibirsk: Nauka, 1977.
- Shebalin, N.V., Macro seismic data as information on source parameters of large earthquakes, *Phys. Earth Planet. Inter.*, 1972, vol. 6, no. 4, pp. 316–323.  
[https://doi.org/10.1016/0031-9201\(72\)90016-7](https://doi.org/10.1016/0031-9201(72)90016-7)
- Shteinberg, V.V., Saks, M.V., Aptikaev, F.F., et al., Methods for setting seismic effects, in *Voprosy inzhenernoi seismologii, vyp. 34: Zadanie seismicheskikh vozdeistvii* (Engineering Seismology Issues, vol. 34: Setting of Seismic Effects), Moscow: Nauka, 1993, pp. 5–94.
- Trifonov, V.G., *Neotektonika Evrazii, Tr. Geol. inst. RAN, vyp. 514* (Neotectonics of Eurasia, Trans. Geol. Inst. RAS, vol. 514), Moscow: Nauch. mir, 1999.
- Ufimtsev, G.F., *Morfotektonika Evrazii* (Morphotectonics of Eurasia), Irkutsk: IGU, 2002.
- Zemletryaseniya Rossii v 2018 godu* (Earthquakes in Russia in 2018), Obninsk: FITS EGS RAN, 2020.
- Zorin, Yu.A., Turutanov, E.Kh., Kozhevnikov, V.M., Rasskazov, S.V., and Ivanov, A.I., The nature of Cenozoic upper mantle plumes in East Siberia (Russia) and Central Mongolia, *Russ. Geol. Geophys.*, 2006, vol. 47, no. 10, pp.1046–1059.

Translated by M. Nazarenko